5-2-2018

Characterizing a Novel Forward Locomotion Mutant in Caenorhabditis Elegans

Christian A. Randall
Georgia State University

CHARACTERIZING A NOVEL FORWARD LOCOMOTION MUTANT IN CAENORHABDITIS ELEGANS

by

CHRISTIAN RANDALL

Under the Direction of Walter W. Walthall, PhD

ABSTRACT

C. elegans provides a number of tools for understanding cellular networks and neural connections. We identified *jd1500* in previous reports as a mutation that affects forward locomotion, which is unusual. Our aims were to: 1) identify the gene responsible for the phenotype that *jd1500* exhibits and 2) distinguish the basis for the locomotive asymmetries. Using next-gen whole genome sequencing, we were able to identify specific genes that are likely responsible for the phenotype it shows. Our results suggest that gap junction mutations mask *jd1500* activity, but also suggest that *jd1500* masks *acr-2* activity.

INDEX WORDS: Proprioception, Gap Junctions, *C. elegans*, *jd1500*, Neural Development.

CHARACTERIZING A NOVEL FORWARD LOCOMOTION MUTANT IN CAENORHABDITIS ELEGANS

by

CHRISTIAN RANDALL

A Thesis Submitted in Partial Fulfillment of the Requirements for the Degree of

Master of Science

in the College of Arts and Sciences

Georgia State University

2018

CHARACTERIZING A NOVEL FORWARD LOCOMOTION MUTANT IN CAENORHABDITIS ELEGANS

by

CHRISTIAN RANDALL

Committee Chair: Walter Walthall

Committee: Barbara Baumstark

Chun Jiang

Electronic Version Approved:

Office of Graduate Studies

College of Arts and Sciences

Georgia State University

May 2018

DEDICATION

I'd like to dedicate this paper to my mother and father, Maureen and Lawrence. Without them, I would neither exist nor have made it this far. I'd also like to dedicate this paper to coffee. I'm fairly sure I wouldn't have finished it without that elixir.

ACKNOWLEDGEMENTS

As far as acknowledgements go, I've got to give special acknowledgements to Dr. Walthall. There was a point in the initial data analysis where I honestly didn't think I'd actually be doing this as a thesis paper. To write a thesis was my goal from the very beginning and Dr. Walthall actually encouraged me to pursue it when I thought I couldn't. I'd also be remiss if I didn't mention my lab mates, both former and current: Richard, Aaron, Michael, Ling, Xiaobei, Linzie, and Jessie. You guys will probably never read this, but thanks for making the lab a fun environment to work in.

I'd also like to acknowledge Dr. Baumstark and the Biobus crew, for providing a great workplace separate from my lab work. Also, I'd like to thank both Dr. Baumstark and Dr. Jiang for their input on my committee. Then there's Dr. Cymbaluk who graciously allowed me to use his lab equipment to complete my experiments, and Nicolette Dutken with Thermofisher, who walked me through the process for sorting sequencing data. Finally, I want to acknowledge my best friend, Lyndon, who isn't a biology student but helped me sort a huge portion of my data for analysis.

Thank you for your help. You guys are the best.

TABLE OF CONTENTS

LIST OF TABLES

LIST OF FIGURES

1 INTRODUCTION

1.1 Neurons and the Cellular Networks that form them

Cellular networks provide intercellular communication tools that allow groups of cells to adapt to their environment together. Cellular networks are the sum total of a number of 'moving parts': the cells themselves, proteins both on the surface of and within the cell, specific molecules necessary for protein activity, and various nucleic acids. Of the cellular networks, neural networks are arguably the most important. Neural networks are formed between a combination of interconnected neurons and other neurons or non-neural target cells (Foster et. al., 1897). Neural communication is integral parts of a variety of systemic functions that include are not limited to nociception in dermal cells, memory formation, and locomotion. In most animal species, locomotion involves interconnected neural and muscular networks. Neural connections between both neurons and muscle cells are referred to as synapses, of which there are two kinds (Foster et. al, 1897; Fitzpatrick et al., 2001).

Chemical synapses are a specialized cellular communication tool that allows neurons to communicate with each other and with muscle cells. They are characterized by synaptic clefts, which are small gaps between the communicating cells that allow the transmission of neurotransmitters (Fitzpatrick et al., 2001). Within the synaptic cleft are a few functional parts on both the presynaptic and postsynaptic cell. The presynaptic cell contains neurotransmitter vesicles and cellular machinery that facilitates vesicular release on its axonal end (Fitzpatrick et al., 2001). The postsynaptic cell has receptors on its dendrite that bind to the neurotransmitter released by the axon of the presynaptic cell (Fitzpatrick et al., 2001). Also found in the dendrite of the postsynaptic cell is a complex of intercellular anchoring and trafficking proteins—the post synaptic density—that allow the postsynaptic cell to modulate the number of available receptors

for neurotransmitters (Fitzpatrick et al., 2001). Neurotransmitters modulate the activity of the postsynaptic cell in one of two ways: by attaching to gated ion channels or by modulating the activity of second messenger pathways within the cell (Fitzpatrick et al., 2001). Because of the small length of 20 to 40 nm found in the synaptic cleft, neurons involved can quickly alter the concentration of neurotransmitters by releasing more or increasing re-uptake of released neurotransmitters (Fitzpatrick et al., 2001). In this way, chemical synapses control the firing of neural action potentials.

Some neurons use both chemical synapses and electrical synapses. Termed gap junctions, these electrical synapses are formed by multi-subunit pores between two adjacent cells (Hu et. al., 1999). These are approximately 3.5 nm in length and allow ions and other small molecules to pass between cells without using neurotransmitters. In neurons, gap junctions allow electrical impulses to pass between cells, which helps propagate action potentials (Hu et. al., 1999). In vertebrate animals, gap junctions are called connexins. These share no sequence similarity with innexins, which are the invertebrate equivalent and are expressed in *C. elegans* (The *C. elegans* Sequencing Consortium, 1998). There are a number of innexins expressed in *C. elegans*, of which a few are functionally related to locomotion (Barnes et. al., 1997; Phelan et. al., 2001; Starich et. al., 1993). Because electrical synapses do not use neurotransmitters, they are not as readily alterable as the chemical synapses (Fitzpatrick et al., 2001). However, due to the direct linkage of the cytoplasm via gap junctions, electrical synapses provide a faster response between the two involved cells (Fitzpatrick et. al., 2001). Gap junctions also allow cells to mirror each other, with the postsynaptic cell mirroring either the depolarization or hyper polarization of the presynaptic cell (Fitzpatrick et. al., 2001).

Both synaptic controls can contribute to a rhythmic neural system, which allows for precise control of muscular contractions. The cellular networks that are responsible for generation of rhythmic contractions in mammals and other animals are referred to as Central Pattern Generators (Proske et. al., 2009). CPGs use proprioceptive elements to manage muscle tension and tone in rhythmic contractions. They do this by detecting the positioning and velocity of a muscle (Proske et. al., 2009; Prochazka et. al., 2007). Proprioceptive feedback in mammals involves a combination of vestibular neurons, eyes, joint, and stretch receptors located in the muscle of the animal (Proske et. al., 2009). This feedback system can mediate both extension and flexion in antagonistic muscle groups, allowing an animal to fine tune its muscle use to its terrain (Proske et. al., 2009). Insight for the mechanism has been found in many animal species, including the mouse and the cat. The cat, in particular, alters its muscle activation patterns during walking in response to the pitch of its head (Gotschall et. al., 2007). Proprioceptive reflexes found in the neck of the cat activate when the head of the animal is tilted upward or downward while parallel to a fixed surface (Gotschall et. al., 2007). Upward tilts caused forelimb flexion and downward tilts caused hindlimb flexion (Gotschall et. al., 2007).

To better understand complex neural networks, simpler neural systems like that of Caenorhabditis elegans are used. *C. elegans* is a tractable model for studies surrounding neural development because the challenges faced in developing its cellular networks are similar to mice and many of its cellular mechanisms are conserved across species. *C. elegans* has a number of advantages that make it a suitable model system. It is a dimorphic species of nematode worms, containing both hermaphrodites and males. The presence of hermaphrodites allows a single animal to generate progeny independent of a mating event. *C. elegans* animals are nearly microscopic, at 1.5 mm on average for an adult hermaphrodite.

1.2 *C. elegans* as a model system

C. elegans worms have a short life cycle that starts as an egg. The animal hatches into its first larval stage from an egg laid by the hermaphroditic mother after sixteen hours. The animal then undergoes the first of four molts to become a young adult (fig 1). This growth can occur as fast as 3 days. Due to the short life cycle and the presence of male/hermaphrodite dimorphism, *C. elegans* can be crossed quickly for genetic screens. Hermaphrodites produce both eggs and sperm, allowing them to self-fertilize in the event that males are not present. In this way, hermaphrodites can create nearly identical genetic copies of themselves. Variation is introduced into a population of hermaphrodites by introducing males, who only produce sperm.

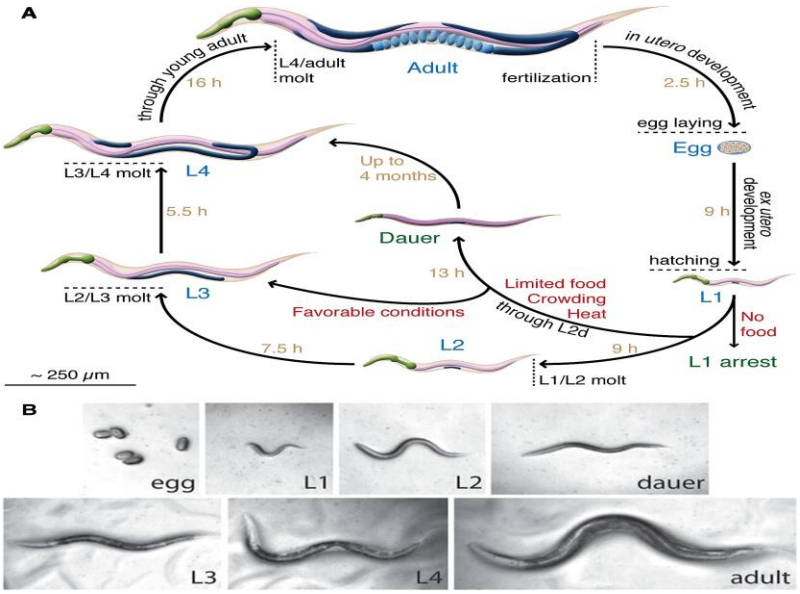

Figure 1 *C. elegans* life cycle (Altun et. al., 2012; Fielenbach et. al., 2008).

The whole genome of *C. elegans* has been sequenced, and many of the genes are homologous to mammalian genes (The *C. elegans* Sequencing Consortium, 1998). This provides an advantage in using this model system in that many insights concerning mammalian genetic activity can be ascertained at a cellular level. Also, every cell has been categorized and all of the lineages have been described. Many of the cellular networks are also well understood, especially

with regards to neuromuscular connections. The locomotion of these animals has been studied extensively, though there is still more to learn. These facts combine to make *C. elegans* a good model system for studying neuromuscular cellular networks and their underlying gene networks.

1.3 The *C. elegans* Nervous System

C. elegans has a small nervous system when compared to complex model organisms like mice and *Drosophila melanogaster*. In total, an adult *C. elegans* hermaphrodite has 302 neurons (Altun et. al., 2013). The nervous system is grouped into classes of neurons defined by their synaptic connections (White et. al., 1986; Altun et. al., 2013). For example, mechanosensory neurons such as ALM and PLM are defined by their connection to the surface of the animal, which allows them to respond to stimuli applied to the "skin" of the animal (Chalfie et. al., 1985).

The cell bodies of seventy-five motor neurons are grouped along the ventral side of the animal. There are eight different classes of motor neurons: AS, DA, DB, DD, VA, VB, VC, and VD. The location of the neuromuscular junction denoted by 'D_' for dorsal and 'V_' for ventral. On the dorsal side, there is a dorsal nerve cord that consists of neurites that extend from the ventral processes via commissures that allow the "D_" motor neurons of each class (Altun et. al. 2013).

The A-, AS and B motor neurons produce acetylcholine and stimulate body wall muscle cells. The D motor neurons produce GABA (gamma-amino butyric acid) and inhibit body wall muscle cells (White et. al., 1976; Chalfie et. al., 1985). Along with the motor neurons are five interneuron classes that innervate the A- and B- motor neurons in a type-specific manner. Interneurons that directly influence motor neurons include AVB, PVC, AVA and AVD/E (Chalfie et. al., 1985). AVB neurons provide stimulus via gap junctions between them and the B

motor neurons while PVC uses chemical synapses to do the same (Altun et. al, 2013). The B motor neurons propagate forward locomotion while the A- and D- motor neurons propagate backward locomotion (White et. al., 1976). AVA uses both chemical synapses and gap junctions while AVD/E uses just chemical synapses to stimulate A motor neurons (Altun et. al, 2013). Innervating those interneurons is the aforementioned ALM and PLM neurons that respond to external stimuli (Chalfie et. al., 1985). These neural connections attach to four muscle strands that span the length of the animal. The two dorsal strands contract in synchrony and the two ventral muscle strands contract in synchrony but because of the cross-inhibitory network established by the VD and DD motor neurons, the dorsal and ventral muscle strands conduct contractile waves that are 180^{o} out of phase with one another. These cellular networks allow the animal to move forward and backward in a rhythmic, sinuous motion due to continuous waves of muscle contraction that run from anterior to posterior when the animal moves forward and posterior to anterior when the animal is moving backward.

1.4 Aims of this study

The B motor neurons propagate forward locomotion while the A- and D- motor neurons propagate backward locomotion (White et. al., 1976). *jd1500,* first described by Alcala and Walthall, (2015), has an uncoordinated coiler phenotype that specifically affects forward locomotion. Forward locomotion is generally considered to be less susceptible to mutation due to the reduced number of uncoordinated mutants that affect forward locomotion alone as compared to backwards locomotion. This mutation shows a variance in coiling bias, with ~70% of all forward coils occurring on the ventral side of the animal and ~30% occurring on the dorsal side, indicating that the mutation causes a locomotive asymmetry that can affect either side of the animal (Alcala, 2016).

All VNC motor neuron cell bodies are present based on prior experiments (Alcala, 2016). Analysis of double mutants for *unc-4*, *unc-25*, and *unc-4*2 suggested that the mutation is not localized to the DA/VA, DD/VD, or AVA/D/E neuron networks, respectively (Alcala, 2016). *unc-4* codes a homeobox protein necessary for the identity of A motor neurons (Miller et. al., 1992). *unc-25* codes glutamic acid decarboxylase, which is necessary for DD/VD activity (McIntire et. al., 1993). *unc-4*2 codes a paired homeodomain necessary for AVA/D/E fate specification (Baran et. al., 1999). Interpretation of these data suggested the DB motor neurons are the targets of this mutation, though more study is needed due to this being a negative result. Mapping data showed that it is an X-linked defect mapped between -9.42 cM and -11.73 cM (Alcala, 2016).

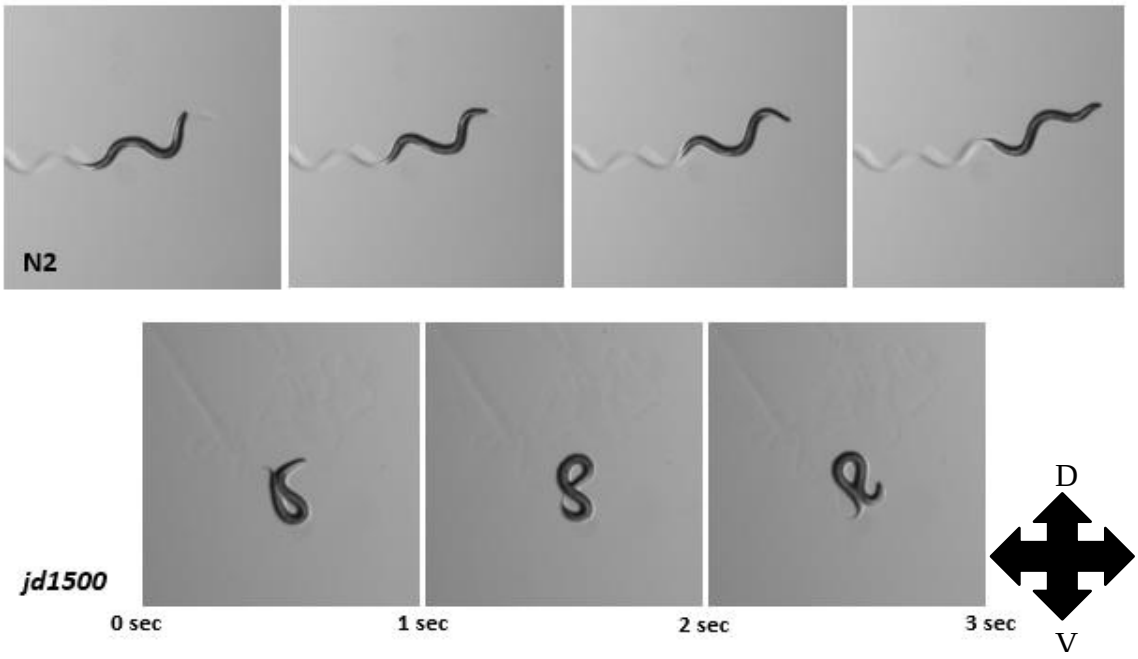

Figure 2 *jd1500* coiling behavior. Compared against wild-type (adapted from Alcala et. al, 2016).

We tested two hypothetical explanations for the cellular basis of the *jd1500* uncoordinated phenotype. Our first hypothesis was that the mutation affects the nematode's proprioceptive feedback system, which for forward locomotion has been shown to involve the B motor neurons. Previous research demonstrated that proprioceptive coupling of B motor neurons is necessary for the generation of the sinusoidal body wave (Wen et. al., 2012). Our second hypothesis posited that the mutation affects the gap junctions that are between the B motor neurons and the PVC/AVB interneurons (Kawano et. al. 2011). In this study, we aim to 1) identify the specific gene associated with the *jd1500* phenotype and 2) distinguish the basis for the locomotive asymmetries.

2 EXPERIMENT

2.1 Strain Maintenance and Mating Protocol

The following alleles were used for experimentation: *acr-2* (ok1887), *ceh-63* (UL2652 ,UL2651), *jd1500*, *unc-7* (e5), *unc-9* (e101), *sax-1* (ky211), *tag-52* (ok1072), *trp-4* (sy695), and *vab-7* (e1562). Alleles for *ceh-63* were obtained from the Ian Hope lab at the University of Leeds. All other strains, with the exception of *jd1500*, which was generated in our lab, were obtained through the Caenorhabditis Genetics Center (CGC). N2 Bristol was used as the wild-type strain. All strains were maintained on NGM plates with a lawn of OP50 *E. coli* according to the protocol outlined in Brenner (Brenner, 1974).

Matings were performed in order to generate double mutants and for complementation tests. For these matings, *jd1500* males were obtained by mating five N2 males with two *jd1500* hermaphrodites. In the F1 generation, males showing the forward coiler phenotype were selected and used for further matings. To ensure successful crosses using *jd1500* males, between ten and fifteen males expressing the *jd1500* phenotype were plated with two L4 to young adult hermaphrodites. These matings were checked at day 3 for young male offspring and screened on day 4.

For complementation tests, the following mutants were used: *ceh-63*, *sax-1*, and *tag-52*. Each mutant was crossed according to the mating protocol listed above. For these crosses, the F1 generation was screened for male progeny to confirm success, then hermaphrodites showing either wild-type or forward uncoordinated locomotion. For *ceh-63*, data from both alleles was combined. For double mutant generation, all other strains were used. These were screened in the F1 generation for wild-type behavior. Wild-type animals were then isolated and allowed to self-fertilize. In the F2 generation, animals were screened to identify and isolate double mutants.

2.2 Whole genome sequencing

Whole genome sequencing was performed with assistance from the CORE facilities at GSU. The *jd1500* genome was isolated by Aaron Alcala using a genomic DNA prep protocol developed by the Hobert lab. The Gentra Puregene kit by Qiagen was used to collect a sample and the sample was tested for purity using a spectrophotometer. Samples were sequenced using the Ion PGM System Next-Gen. Sequencer. The *jd1500* genomic sequence was compared to the WB235.75 *C. elegans* genome sequence obtained using the Ion Torrent client. Data were analyzed using excel databases developed in GALAXY to identify the defective locus (Enis et. al. 2016). Data obtained through sequencing was constrained by the region identified in the deficiency mapping experiment. Higher priority was placed on genes that had internal deletions or non-synonymous polymorphisms within an exon region. Genes expressed in the VNC motor neurons or the motor circuit interneurons were prioritized. From this analysis, a list of likely candidates for the *jd1500* allele was developed.

2.3 Locomotion assays

2.3.1 Coil Frequency Assay

L4 Hermaphrodites were used for locomotion assay. This was done to remove the presence of eggs as a variable for locomotion. Animals used in assays include: *jd1500, acr-2, unc-7, unc-9, vab-7, trp-4, jd1500 acr-2, jd1500 unc-7, jd1500 unc-9, jd1500; vab-7*, and *jd1500; trp-4*. Animals were transferred to an unseeded plate for all locomotion assays. To determine the coil frequency of each strain, animals were agitated via either by prodding the tail of the animal with a pick, or by dropping the plate from 10-15 cm. The animals were then allowed to move freely for one minute and each forward coil was recorded.

2.3.2 DV Ratio Analysis

To determine the dorso-ventral ratio of the animal, videos were recording for individual animals from each strain using the Leica MZ 16 FA microscope provided by the Cymbaluk lab at GSU. Analysis of dorso-ventral ratios was performed according to procedure outlined in Oommen (Oommen, 1999). For each individual animal, analysis was performed on no more than 5 forward locomotion events. Forward locomotion events are defined as an animal's forward movement lasting between 2-3s, without any pauses or backward movements. Videos were then sorted into 1s portions, which were then clipped in order to view animal forward locomotion in 0.25s intervals. The animals were then examined using the dorsoventral (DV) ratio technique, measures asymmetry between the forces generated by the dorsal and ventral muscles. The DV ratio measures the length of a line produced at a right angle between two body bends (Fig. 3; Oommen, 1999). The line is set at the furthest point within the measured area. Those measured values would be assigned as dorsal or ventral depending on whether it was measured for the dorsal side or the ventral side. Ratios were developed by dividing the ventral side from the dorsal side, which gives a value greater than 1 for animals with a dorsal bias and a value less than 1 for animals with a ventral bias. Animals were not evaluated in the tail region past the preanal ganglion. This was done to remove the non-muscular and non-neural portions of the animal from the analysis, as it would provide an inaccurate representation of the animal's bias.

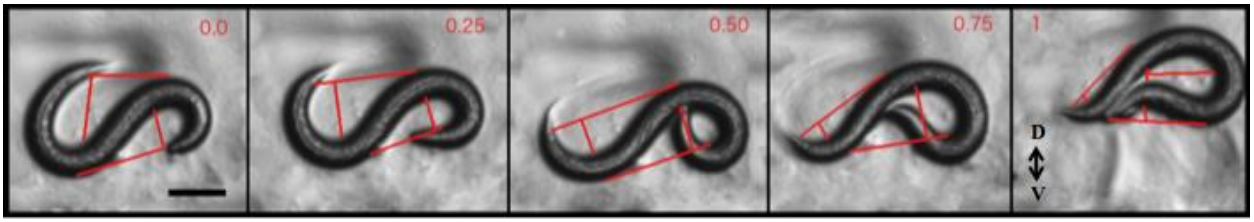

Figure 3 *jd1500* DV Ratio analysis example. Scale Bar represents 101 μm

2.3.3 L1 Bias Analysis

jd1500 L1 animals were also observed to determine the directionality of the coil in young animals. For this, individual worms were isolated and tested under a dissecting scope. Animals were touched on the tail and each coil was scored according to whether it was ventral or dorsal.

3 RESULTS

3.1 Next-Gen Whole Genome Sequencing and Genetic Screening

To learn more about the genetic aberration responsible for the *jd1500* allele, we employed next-gen whole sequencing techniques. Genomic DNA was isolated by Aaron Alcala using the Gentra Puregene Kit. The sample was pure, at 260/280=1.85, where anything below 1.8 is considered impure. Raw Genomic DNA was then sequenced by the CORE facilities using the Ion torrent DNA sequencer. Genome sequences were compared against the N2 Bristol strain. The total number of sequenced base pairs was 6.87 G. The sequence underwent 58,252,270 total reads, of which 55,103,047 reads were aligned, giving an approximate 92% read coverage. A mean raw accuracy of 98.8% was found at a read length of approximately 128 bp. This indicates that most of the genome was read, and that the read sections are accurate (Fig. 3).

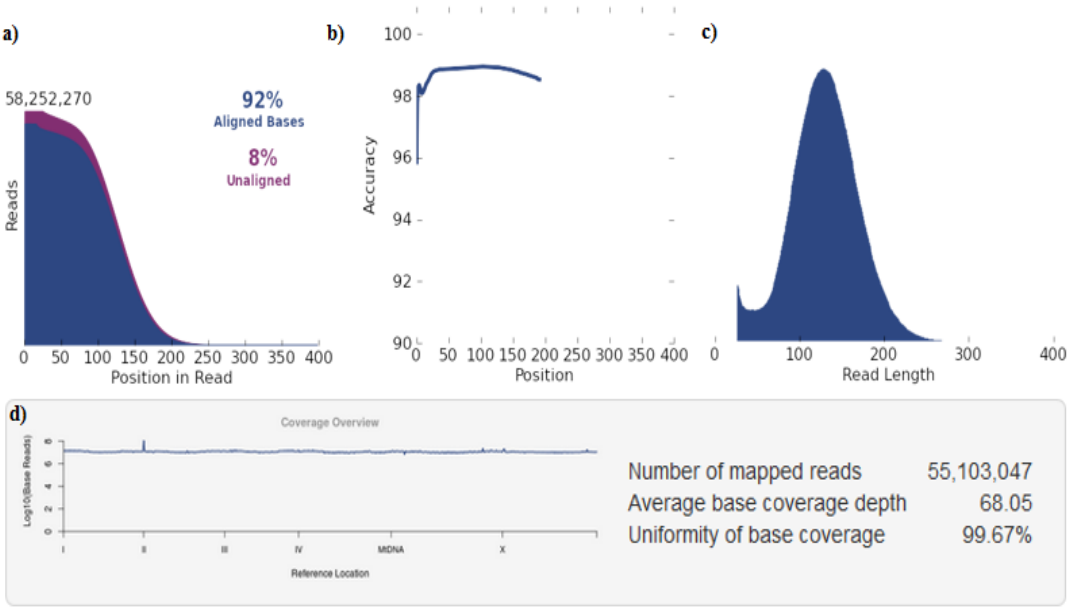

Figure 4 Data from Ion Server. a) Read coverage. b) Accuracy across different read lengths c) Histogram of read lengths that provided most accurate reads. d) Mapped reads, Base coverage depth, and uniformity of base coverage.

Before beginning analysis, the data were introduced into GALAXY (Enis et. al. 2016). GALAXY has a number of tools that simplify analysis of genomic data. All data can be exported to Microsoft Excel for sorting. For our work, only two tools were used: snpEFF and VCFsort. The tool snpEFF allows users to sort aligned genomic data based on the known aberrations found on each chromosome. This method of sorting lists data in numerical order based on base pair positions. It also provides an expected genomic effect. VCFsort takes the same data and sorts it based on gene name. VCFsort allows users to search for specific genes and review the gene for any effects that are given their own category. While snpEFF provides statistical likelihood of effect with terms like HIGH or MODERATE, VCFsort lists just the numerical values like the position on the genome. Used in tandem, these tools can provide insight into all potential mutations.

Given that the mutation is on the X chromosome, and located in an interval covered by the deficiency, which covers from -9.42 to -11.73 cM, Within this region, nineteen genes had been identified by mutant phenotype (Table 1). Of those genes, higher priority was placed on genes that have mutations within identifiable exon regions and that are expressed within the neuromuscular network. Two mutations, *ceh-63* and *tag-52*, were found at -9.43 cM and -9.83 cM, respectively, that fit the aforementioned criteria (table 1).

Table 1 Candidate genes found within the deficiency region. Gene descriptions are sourced from wormbase.org. Stars indicate genes that have been tested. Genome effect data is sourced from analysis.

Gene	Location (cM)	Known Phenotypes	Genome effect data
ceh-18	-9.28 +/- 0.025	Larval lethal	Intron variant, 1 bp
lim-4	-9.21 +/- 0.025	Dauer formation variant, Butanone Chemotaxis variant	Stop gained, 1 bp
sup-12	-9.17 +/- 0.056	Body Wall Muscle Morphology variant	Upstream Gene variant, 1 bp
fkh-9	-9.33 +/- 0.020	n/a	Downstream gene variant, 14 bp

rgl-1	-10.75 +/- 0.016	Indirect – Organism Development variant	Intron variant, 1 bp
C18B2.2	-9.95 +/- 0.000	n/a	Downstream gene variant, 22 bp
mir-271	-10.34 +/- 0.000	MicroRNA mutation	Upstream Gene variant, 1 bp
dhs-26	-10.42 +/- 0.000	n/a	Intron variant, 1 bp
clc-3	-10.40 +/- 0.020	Body wall myosin organization defect	Upstream Gene variant, 1 bp
rgs-7	-10.11 +/- 0.034	n/a	Missense variant, 1 bp Intron variant, 1 bp
ckc-1	-10.03 +/- 0.000	Reduced brood size	Missense variant, 1 bp
sax-1*	-9.91 +/- 0.019	Axon outgrowth variant Ectopic Neurite outgrowth	Upstream Gene variant, 1 bp
ceh-63*	-9.84 +/- 0.000	n/a	Upstream gene variant, 41 bp
tag-52*	-9.83 +/- 0.014	n/a	Frameshift mutation, 41 bp
gbb-1	-12.67 +/- 0.001	Acetylcholinesterase inhibitor hypersensitive Aldicarb hypersensitivity	Intron variant, 100 bp
dhs-27	-10.34 +/- 0.000	n/a	Intron variant, 1 bp Upstream Gene variant, 1 bp
sox-4	-10.25 +/- 0.008	n/a	Downstream gene variant, 1 bp
fax-1*	-10.75 +/- 0.120	Axon guidance variant, axon regeneration defective, locomotion variant.	n/a
unc-78*	-10.34 +/- 0.003	Actin organization biogenesis variant, aldicarb resistant, body wall muscle sarcomere variant, locomotion variant.	Synonymous variant, 1 bp Upstream gene variant, 1 bp
sax-3*	-10.34 +/- 0.008	Axon guidance variant, axon outgrowth variant, alm migration variant, kinker.	Dowstream Gene variant, 1 bp
unc-20*	-11.61 +/- 0.197	Kinker, coiler, axon outgrowth variant, head muscle contraction variant.	n/a

spc-1*	-12.14 +/- 0.054	Aldicarb resistant, dumpy, locomotion variant.	n/a
wrt-6*	-10.31 +/-0.015	Body vacuole, intestinal vacuole, locomotion variant.	n/a
fkh-2*	-9.5 +/- 0.044	Embryonic lethal, L1 arrest, sluggish	n/a
dop-1*	-7.65 +/- 0.029	Backward Locomotion, forward locomotion decreased, head bend angle variant, locomotion variant.	n/a
unc-2*	-13.79 +/- 0.063	Backward locomotion variant, aldicarb resistant.	n/a

At -9.43 cM, we identified an upstream gene mutation of 41 bp in *ceh-63* (table 1). *ceh-63* encodes a homeobox protein that is similar to vertebrate Hox3 proteins and to the *D. melanogaster* HOX protein ROUGH (Feng et. al., 2012). *ceh-63* is expressed in hermaphrodites in two cells: primarily in DVC and a vulva cell found separate from the uterus (Feng et. al., 2012). DVC is a stretch receptor neurons that is thought to be necessary for backward locomotion (Feng et. al., 2012). Phenotypically, it is incompletely penetrant, showing variations of forward and backward coiling in its population ranging from completely paralyzed to freely moving.

At -9.83 cM, we identified a frameshift mutation caused by an internal deletion of 41 bp in the gene *tag-52* (table 1). This mutation was flagged as 'HIGH' in the snpEFF data. *tag-52* encodes a protein that is predicted to have Rho-guanyl exchange factor activity (Ziel et. al., 2009). It is an ortholog of human ARHGEF39 that is expressed in the nervous system, pharynx, and reproductive system of *C. elegans* (Spencer et. al., 2010; Ziel et. al., 2009). *tag-52* has no locomotion phenotype. Using modENCODE, we were able to confirm that the mutation is on the fifth exon, deleting the amino acid sequence 'MPLCKYEPSA' starting at amino acid 296

(Celniker et. al., 2009). *tag-52* is directly upstream of *ceh-63*, and the data from the snpEFF confirmed that the deletion in *tag-52* causes the frameshift in *ceh-63*.

Using the insights we gained from the genome analysis, we set up complementation tests for *tag-52*, *ceh-63*, and *sax-1*. Due to data from the genomic analysis, we hypothesized that the phenotype in *jd1500* is caused by a mutation in *tag-52*. Of the three genes tested, all genes complemented *jd1500*. This suggested that neither of these genes were responsible for the mutant phenotype of *jd1500*.

3.2 Locomotion Assays

3.3.1 L1 Bias Testing

We wanted to confirm that L1 animals had a similar pattern of ventral bias to older animals. To do this, we tested individual animals on their forward locomotion response to light touch. In the five animals tested, we saw a similar ratio of 24% dorsal to 76% ventral bias. This suggested that the defect is likely caused in embryonic cells. This lends credence to the hypothesis that embryonic cells are the cells primarily affected by the mutation.

3.3.2 Proprioceptive Mutant Analyses

We then performed locomotion assays on animals. For these, L4 to young adult animals were chosen. Double mutants were tested for gene interactions. Epistasis describes a gene interaction scenario in which one of the two mutant phenotypes masks the second phenotype in the double mutant. We tested the locomotion patterns of selected double mutants, first to determine whether the animals displayed any differences in the frequency of the coiling behavior. For this experiment, a coil was counted if the head of the animal touched the midbody of the animal near its vulva when attempting forward movement.

To analyze interactions between *jd1500* and proprioception we tested double mutants of *jd1500* with *acr-2, vab-7,* and *trp-4*. Each of these mutations is necessary for proprioceptive feedback of *C. elegans* (Li et. al., 2006; Wen et. al., 2016). *acr-2* encodes a nicotinic acetylcholine receptor that creates a channel when coexpressed with *unc-38*. It is expressed across the *C. elegans* motor circuit. In particular, *acr-2* is expressed in the B motor neurons, which are responsible for forward locomotion. *acr-2 (ok1887)* has a mild backward locomotion phenotype, in which it backs faster than controls, as well as increased head bend angles and increased nose movement. *jd1500 acr-2* exhibited forward coiling similar to *jd1500,* however the increased nose movement can be observed. The *jd1500* single mutant had a coil frequency of 5.8 coils per minute and the *acr-2* single mutant had a coil frequency of 0.267 coils per minute, which were not statistically similar (p=0.0001). *jd1500 acr-2* had a coil frequency that is statistically similar to *jd1500,* at an average of 5.53 (p=0.764) coils per minute (Fig. 5). However, when compared against *acr-2,* it exhibits a significantly higher coil frequency (p=0.0002). This suggests that *jd1500* is masking *acr-2* in coil frequency measurements.

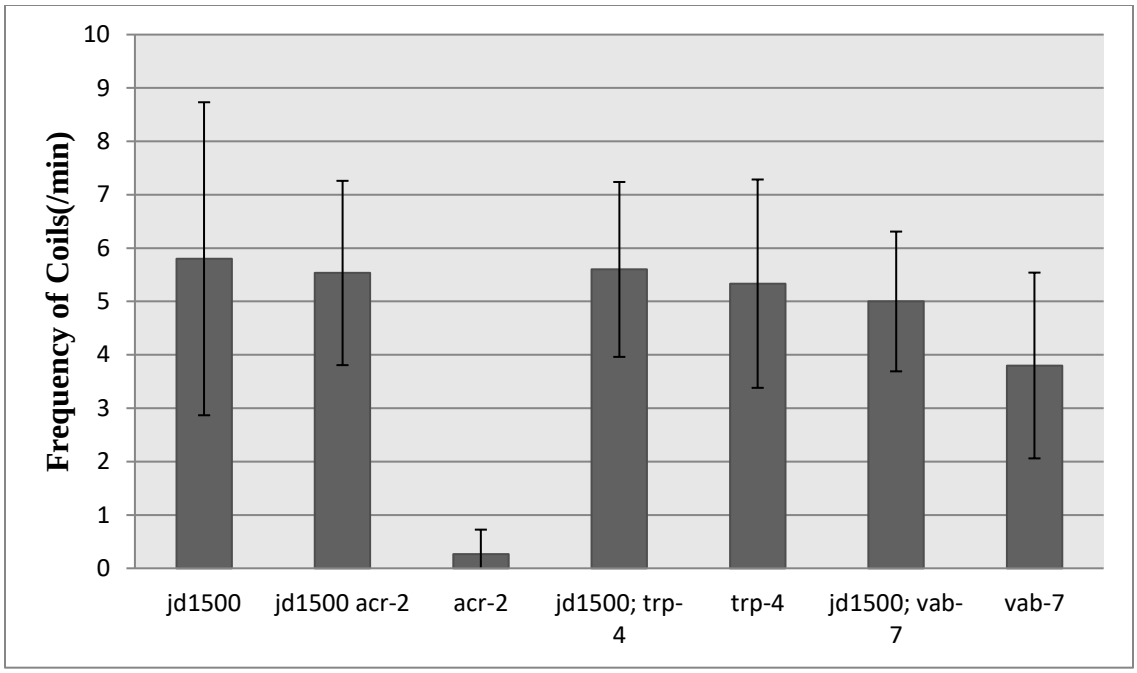

Figure 5 Coil Frequency Comparison for *jd1500* and proprioceptive mutants. Error bars represent standard deviation. Significance was calculated using ANOVA. If p-values were less than 0.05 in ANOVA, t-tests were applied to discern which of the tested mutants were similar or not. (n=15) (Table 2)

Next, we observed *jd1500; vab-7* double mutants. *vab-7* encodes a homeodomain protein that is responsible for DB motor neuron identity (Esmaeili et. al., 2002). In mutants of *vab-7*, locomotion defects can be observed. Animals exhibit a larger amplitude of sinuous motion when compared against wild type animals (Esmaeili et. al., 2002). *vab-7* mutants also exhibit various morphological defects localized to the tail region. These can range from a truncated tail to a tail with blisters. These physiological defects can hamper backward locomotion in these animals. *jd1500; vab-7* exhibits forward coiling, with the morphological differences acting as a marker for *vab-7*. The *jd1500* single mutant had a coil frequency of 5.8 coils per minute and the *vab-7* single mutant had a coil frequency of 3.8 coils per minute, which were not statistically similar (p=0.033) (Fig. 5). The *jd1500*; *vab-7* double mutant had a coil frequency of 5 coils per minute,

which was statistically similar to both *jd1500* (p=0.346) and *vab-7* (p=0.055). This suggests that *vab-7* is not masking *jd1500* in coil frequency measurements.

Finally, we tested *trp-4*. *trp-4* encodes a subunit of a TRPN channel that acts as a pore for that channel (Li et. al., 2006). It is specifically expressed in the DVA interneuron, which is an important interneuron that acts as a stretch receptor for forward locomotion. It is also expressed in the DVC a single interneuron thought to be necessary for backward locomotion. *trp-4* is required for proprioception in *C. elegans* that is controlled by stretch receptors (Li et. al., 2006). Single mutants of *trp-4* exhibit increased amplitude of sinuous motion similar to *vab-7*. *trp-4* mutants can move backwards where *vab-7* sometimes cannot, but this movement also exhibits the same increased amplitude. Double mutants of *jd1500* and *trp-4* exhibit forward coiling. *jd1500; trp-4* also exhibits backward coiling, where *jd1500* did not. The *jd1500* single mutant had a coil frequency of 5.8 coils per minute and the *trp-4* single mutant had a coil frequency of 5.33 coils per minute, which were statistically similar (p=0.849). The coil frequency of *jd1500; trp-4* was statistically similar to *jd1500*, with an average coil frequency of 5.6 (p=0.849) coils per minute (Fig. 5). This suggested that *trp-4* is not masking *jd1500* in coil frequency measurements.

We further tested the whether *jd1500* is masked by proprioceptive mutants by recording videos of each mutant for comparison and gathering DV ratios. This method was used because it provided an approximation of differential coiling behavior between animal populations that can be quantified. For this set of experiments, we chose 6-8 animals from each genotype, recording and analyzing no more than 5 coils from each animal. We chose not to examine *vab-7* using this method because it exhibits a morphological defect in addition to its neurological defect that could potentially provide erroneous information about its coiling behavior when compared to *jd1500* using this method. For the animals tested, we then sorted the locomotion events by

whether they coiled toward the dorsal side or the ventral side of the animal. Due to the smaller sample size of dorsal coils, we chose to focus on ventral coils. The critical differences arose at the 0.75s and 1s mark for most animals tested, so we focused on that portion of the data for statistical analysis.

Interactions were assumed if a statistically significant difference was observed between *jd1500* and tested double mutants using t-tests. DV ratios for each of the single mutants were also determined for comparative purposes. To determine whether *jd1500* masked the phenotype of those mutants. *jd1500* single mutants had a mean DV ratio of 0.511 at 0.75s and a mean ratio of 0.411 at 1s for ventral coils. *trp-4* single mutants had a mean DV ratio of 0.36 at 0.75s and 0.683 at 1s (Table 3; Fig. 6). *jd1500; trp-4* had a mean DV ratio of 0.547 at 0.75s and 0.594 at 1s (Table 3; Fig. 6). At 0.75s, *jd1500* was statistically similar to both *trp-4* (p=0.355) and *jd1500*; *trp-4* (p=0.776). These similarities also held for earlier points in the time series. These data, taken together with the coil frequency data, suggested that *trp-4* and *jd1500* are similar to each other and that neither single mutant is masking the other.

The next comparison was *jd1500 acr-2* with *jd1500* and *acr-2*. *jd1500* single mutants had a mean DV ratio of 0.511 at 0.75s and a mean ratio of 0.411 at 1s for ventral coils. *acr-2* single mutants had a mean DV ratio of 0.895 at 0.75s and a mean ratio of 0.918 at 1s for ventral coils (Table3; Fig. 6). *jd1500 acr-2* had a mean DV ratio 0.463 at 0.75s and 0.747 at 1s, neither of which was statistically different from *jd1500* at either time point (p=0.689; p=0.071) However, *jd1500 acr-2* showed significant differences when compared against *acr-2* at 0.75s (p=0.0002) (Table3; Fig. 6). Differences in DV ratio between *jd1500 acr-2* and *acr-2* could also be observed at 0.25s and 0.5s. This, in conjunction with coil frequency data, suggested that *jd1500* masked *acr-2*.

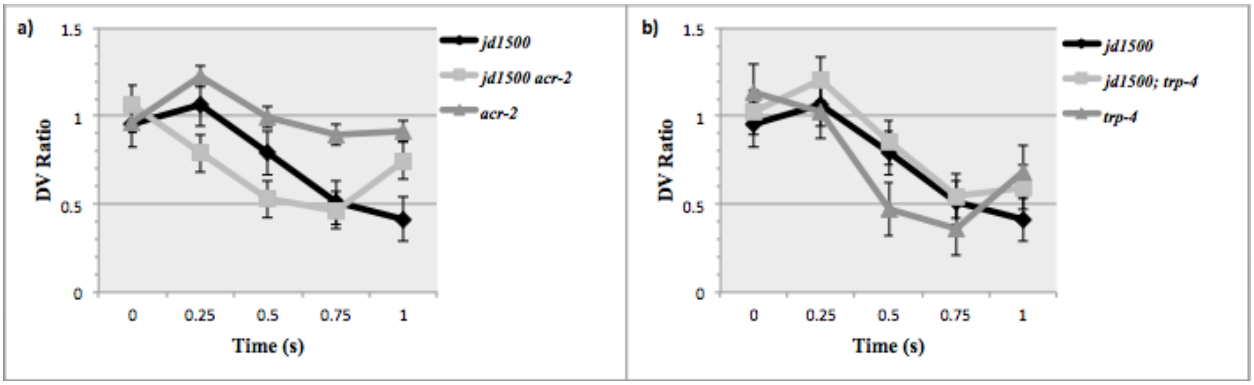

Figure 6 DV Ratio Time Series. Error bars indicate Standard Error. See Table 3 in appendix for values.

a) Ventral Coiling ratio comparison for *jd1500*, *jd1500 acr-2*, *acr-2*.
b) Ventral Coiling ratio comparison for *jd1500*, *jd1500*; *trp-4*, *trp-4*.

3.3.3 Innexin Mutant Analyses

Gap junctions are formed by innexins in *C. elegans (*Kawano et. al., 2011). They act as electrical synapses that facilitate direct intercellular communication between cells. In *C. elegans*, there are a number of innexins that provide connections between the interneurons and specific classes of motor neurons (Kawano et. al., 2011). For the DB and VB motor neurons, the relevant innexin genes are *unc-7* and *unc-9*. *unc-7* is localized to the AVB interneuron that synapses onto VB and DB motor neurons. *unc-9* is similar to *unc-7*, but it is localized to PVC rather than AVB. Phenotypically, these animals appear very similar. They both have forward and backward locomotion defects characterized by frequent pauses and uncoordinated motion (kinking). *jd1500 unc-7* mutants revealed no noticeable change in its backward locomotion but coiling when prodded on its tail as the animal attempted to move forward was observed. This can also be seen in *jd1500 unc-9*. Coiling can occur spontaneously, however it takes longer to occur in the double mutants than in *jd1500* single mutants (Fig. 7).

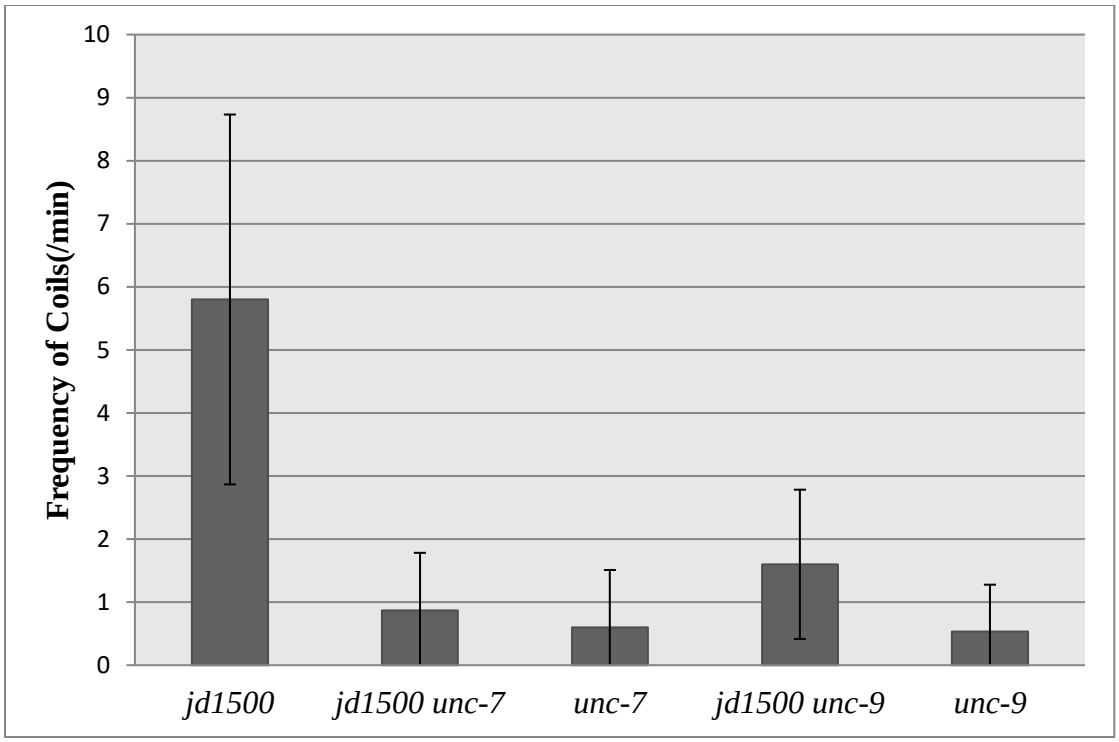

Figure 7 Coil Frequency Comparison for Gap Junction Mutants Error bars represent standard deviation. Significance was calculated using ANOVA. If p-values were less than 0.05, t-tests were employed. (n=15) (Table 5)

The *jd1500* single mutant had a coil frequency of 5.8 coils per minute (Fig. 7). *unc-7* single mutants had a coil frequency of 0.6 coils per minute, while *unc-9* single mutants had a coil frequency of 0.533 coils per minute (Fig. 7). In *jd1500 unc-7* double mutants, the coil frequency averaged 0.867 coils per minute, while in *jd1500 unc-9* double mutants the coil frequency averages 1.6 coils per minute (Fig. 7). Coil frequency analysis of the double mutant *jd1500 unc-7* yielded no statistically significant differences when compared against *unc-7* ($p=0.431$), but did yield significant differences when compared with *jd1500* ($p=0.023$). Coil frequency analysis of the double mutant *jd1500 unc-9* showed statistically significant differences when compared with *unc-9* ($p=0.007$) as well as statistically significant differences when compared with *jd1500* ($p=0.0007$). The difference in the coil frequency data for these double mutants could be attributed to the fact that these innexins mutants primarily affect different cells. These data

suggest that *jd1500* is masked by both *unc-7* and *unc-9* in the frequency of coiling events.

We hypothesized that if *unc-7* and *unc-9* are masking *jd1500*, we should see a significant difference in the DV ratio of *jd1500 unc-7* and *jd1500 unc-9* at 0.75s and 1s when compared to the *jd1500* single mutant, but not when compared against *unc-7* and *unc-9*, respectively. *jd1500* single mutants had a mean DV ratio of 0.511 at 0.75s and a mean ratio of 0.411 at 1s for ventral coils. *unc-9* single mutants had a DV ratio of 0.908 at 0.75s and 0.904 at 1s (Table 6; Fig. 8). *jd1500 unc-9* had a mean DV ratio of 0.849 at 0.75s and 0.741 at 1s (Table 6; Fig. 8). These values were significantly different when compared to *jd1500* at both 0.75s (p=0.014) and 1s (p=0.021) but similar to *unc-9* at 0.75s (p=0.587) and 1s (p=0.207). These data suggested *unc-9* is masking the *jd1500* phenotype and is required for *jd1500* to function (Fig. 8).

Because *unc-7* appeared to have more differences to jd1500 in DV ratios, we chose to examine 0.25s and 0.5s as well. *jd1500* single mutants had a mean DV ratio of 1.07 at 0.25s, 0.792 at 0.5s, 0.511 at 0.75s, and a mean ratio of 0.411 at 1s for ventral coils. *unc-7* exhibited a mean DV ratio of 0.984 at 0.25s, 1.02 at 0.5s, 0.743 at 0.75s, and 0.884 at 1s (Table 6; Fig. 8). *jd1500 unc-7* exhibited a mean DV ratio of 0.553 at 0.25s, 0.484 at 0.5s, 0.522 at 0.75s, and 0.891 at 1s (Table 6; Fig. 8). *jd1500 unc-7* did not have statistically significant differences when compared with *jd1500* at time 0.5s (p=0.076) or 0.75s (p=0.929), which was not expected. It did however have statistically significant differences at 0.25s (p=0.007) and 1s (p=0.036). When compared with *unc-7*, *jd1500 unc-7* had significant ventral biasing at 0.25s (p=0.002), 0.5s (p=0.003), and 0.75s (0.025). When taken in context with the entire time series, *unc-7* mutants appeared to accelerate bias formation for ventral coils (Table 6; Fig. 8).

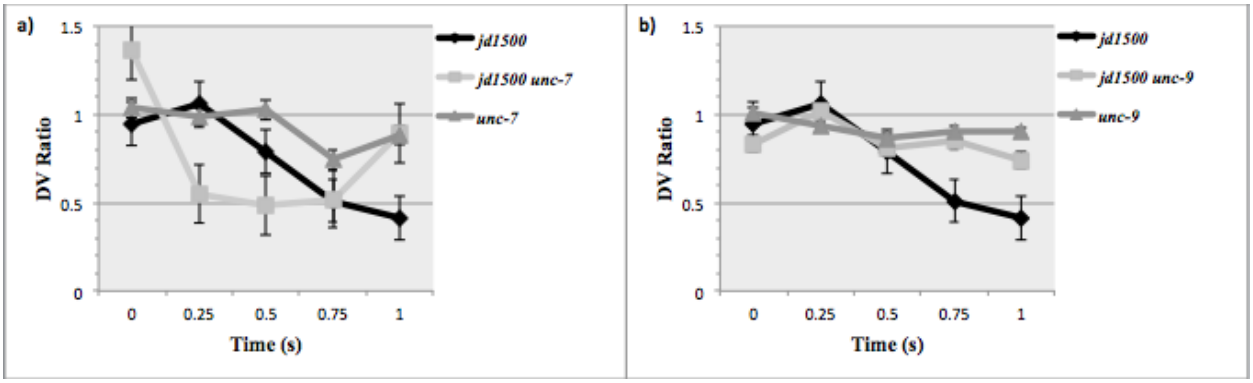

Figure 8 DV Ratio Time Series. Error bars indicate Standard Error. See Table 6 in appendix for values.

a) Ventral Coiling ratio comparison for *jd1500, jd1500 unc-7, unc-7.*
b) Ventral Coiling ratio comparison for *jd1500, jd1500 unc-9, unc-9.*

To further investigate the epistatic interaction between *unc-7* and *unc-9* and *jd1500*, we tested *unc-7* and *unc-9* in an *unc-30* background. Since the gap junction mutants masked the bias of *jd1500,* we asked whether the gap junction mutants would mask other uncoordinated phenotype of *unc-30*. We chose *unc-30* mutants, which have a defect in the release of GABA a critical neurotransmitter involved in proper locomotion. *unc-9* single mutants had a mean DV ratio of 0.908 at 0.75s and 0.904 at 1s. *unc-30* single mutants had a mean DV ratio of 0.595 at 0.75s and 0.676 at 1. *unc-9*; *unc-30* double mutants had a mean DV ratio of 0.614 at 0.75s and 0.587 at 1s. Tests for *unc-9* and *unc-9; unc-30* yielded statistically significant differences at 0.75s (p=0.008) and 1s (p=0.016). Comparisons of *unc-30* to *unc-9*; *unc-30* yielded no significant differences at 0.75s (p=0.882) or 1s (p=0.364). This suggested that *unc-9* did not mask *unc-30* (Table 8; Fig. 9).

unc-7 exhibited a mean DV ratio of 0.984 at 0.25s, 1.02 at 0.5s, 0.743 at 0.75s, and 0.884 at 1s. *unc-30* exhibited a mean DV ratio 0.914 at 0.25s, 0.62 at 0.5s, 0.595 at 0.75s, and 0.676 at 1s. *unc-7*; *unc-30* exhibited a mean DV ratio of 0.791 at 0.25s, 0.585 at 0.5s, 0.641 at 0.75s, and 0.6 at 1s. Statistical tests for *unc-7, unc-7; unc-30,* and *unc-30* yielded no statistically significant

differences at 0.25s (p=0.333; ANOVA) or 0.75s (p=0.447; ANOVA), but did exhibit differences at 0.5s (p=0.031) and 1s (p=0.04; ANOVA) (Table 8; Fig. 9). These differences were tested further using t-tests. *Unc-7* and *unc-7*; *unc-30* showed differences at 0.5s (p=0.043) and 1s (p=0.034). *unc-30* and *unc-7 unc-30* showed no differences at either time point (p=0.85; p=0.523). These data suggested did not mask *unc-30.* These data suggested that *unc-7* and *unc-9* were not necessary for *unc-30* function.

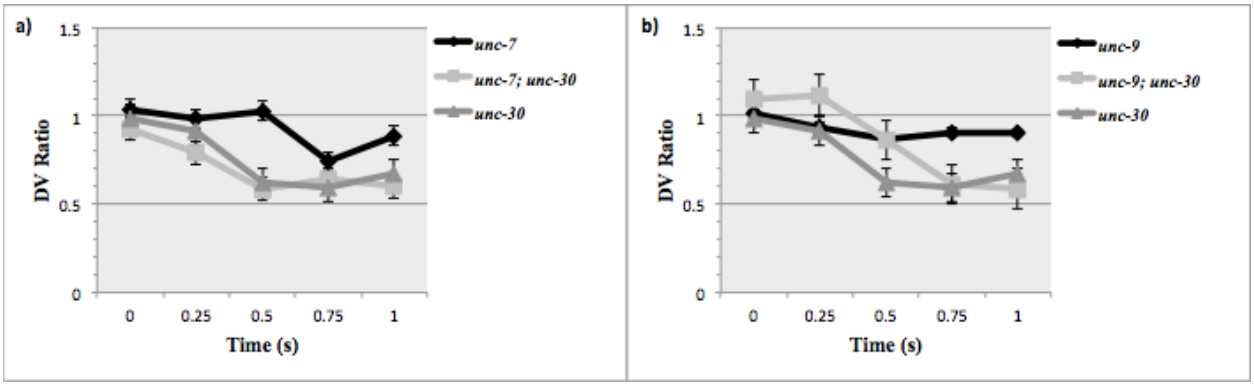

Figure 9 DV Ratio Time Series. Error bars indicate Standard Error. See Table 8 in appendix for values.

a) Ventral Coiling ratio comparison for *unc-7, unc-7; unc-30, unc-30*.
b) Ventral Coiling ratio comparison for *unc-9, unc-9; unc-30, unc-30*.

4 DISCUSSION

Dissecting neural networks is a key component of understanding behavior in a wide variety of animals. Locomotive behavior, in particular, is typically more driven by the neural connections than by the muscular components. Developing models for how these connections are formed and isolating the parts involved presents unique challenges for the scientific community. To attempt to circumvent these challenges, model systems like *C. elegans* are often used. *C. elegans* has a number of functionally similar components to other model systems while being more easily manipulated. Because of the wealth of existing knowledge surrounding *C.elegans* morphology, as well as its genomic data, we can employ a number of techniques to discover more information about the functional components of its neural networks.

4.1 Characterization of the *jd1500* gene

In a previous study, Aaron Alcala identified a deficiency on the X chromosome that failed to complement *jd1500.* He then used complementation testing for seven genes; *dop-1, fax-1, fkh-2, sax-3, unc-2, unc-20,* and *unc-78 (*Alcala, 2016). Mutations in these genes all exhibited forward locomotion phenotypes but all successfully complemented the *jd1500* mutant phenotype. We next employed Next Generation Sequencing (NGS) techniques to learn what gene might be responsible for our mutation. From that data set, a few genes emerged as potential candidates. These genes were given markers for whether they were very likely to be the mutated gene. Of these genes, *tag-52* was given a 'HIGH' likelihood. NGS presents some limitations, however, as it does not say definitively whether a mutated allele is responsible for our phenotype. Two of the mutants studied by Alcala, *unc-78* and *sax-3* were flagged as having SNPs in the NGS data set. We performed complementation tests on *tag-52, ceh-63,* and *sax-1* to determine whether one of those mutants was responsible for the mutant phenotype. All three

genes complemented *jd1500*, which suggested that none were allelic with *jd1500*. This result runs contrary to the NGS experiment, which prompts further testing. Of the genes left in the region, 12 are untested and could potentially be responsible for the *jd1500* phenotype.

In order to more effectively test these genes, as well as the genes that were previously tested, a multiplex PCR technique like Ampliseq or HiSeq should be employed. These are techniques that can be used to genotype a population of animals with similar phenotypes. It has been shown to be useful for identifying genetic variations in a large number of genes per experiment using either DNA or RNA and, with recent advances, can be used with very small amounts of DNA or RNA (Campbell et. al., 2014; Li et.al., 2015). This technique can sort alleles by frequency within the population, with the highest frequency being the responsible gene (Campbell et. al., 2014).

4.2 Characterization of the Gene and Cellular Networks

Forward locomotion is driven by a dedicated set of interneurons, two PVCs and two AVBs that form gap junctions and chemical synapses with a set of motor neurons, the VB and DBs (Bryden et. al, 2008; Fouad et. al., 2018; Kawano et. al. 2011). Two gap junction mutants, *unc-7* and *unc-9*, had been identified that contribute to forward locomotion (Starich et. al., 2009). We found that mutations in *unc-9* were epistatic to the mutant phenotype of *jd1500*. This masking suggested that the *unc-9* innexin was required for the *jd1500* mutant phenotype. In contrast, the DV ratio data for mutants in a second gap junction gene *unc-7* did not mask the forward bias of *jd1500*, but instead actually accelerated the locomotive asymmetries found when the double mutants attempted to move forward (Fig. 8). The difference between these interactions is interesting considering that they are both innexins that mask the *jd1500* phenotype, but in different ways. The key to understanding these differences can be explored

further by looking at *jd1500* in the context of the differences in expression between *unc-9* and *unc-7*. *unc-9* is expressed in the PVC interneurons and B motor neurons. Given that *unc-9* is expressed in the B motor neurons, a candidate class of motor neurons suggested to be targets of the *jd1500* mutation, UNC-9 is preventing the bias control phenotype associated with *jd1500* in these cells (Alcala, 2016).

As mentioned earlier, the PVC functions as a set of command interneurons that are involved in forward locomotion and express UNC-9 innexins. PVC acts as a modulatory element using chemical synapses and gap junctions to suppress activity of the backward locomotion network during forward locomotion (Kawano et. al. 2011). Mutants in *unc-9* disable gap junctions between AVB-B, PVC-AVA, and AVA-A. The effects caused by gap junction disruption in *jd1500* happen alongside undisrupted chemical synaptic activity. PVC also functions as an inhibitory element for the B motor neurons and AVB interneurons via chemical synapses. AVA is generally excitatory to A and AVB is excitatory to AVA (Kawano et. al, 2011; Rakowski et. al., 2013). The gap junctions disabled between PVC and AVA may increase the excitation of AVA and A motor neurons while the gap junctions disabled in AVB significantly reduce the excitation of B motor neurons while the animal is moving forward. These effects, taken together, can explain why *unc-9* masks *jd1500*. If *jd1500* is responsible for synchronous forward locomotion and is expressed in B motor neurons, then decoupling AVB from B and PVC from AVA by removing *unc-9* could mask *jd1500* by significantly reducing the amount of forward locomotion activity and increasing the backward locomotion circuit.

UNC-7 is also altering the bias control phenotype associated with *jd1500*. *unc-7* is not expressed in the B motor neurons or PVC, but in the AVB and AVA interneurons. It is also expressed in some D and A motor neurons. *unc-7* has previously been shown to be involved in

mediating forward locomotion by suppressing the backward locomotion circuit (Kawano et. al., 2011). *unc-7* gap junctions appear to have a modulatory effect on B motor neurons via AVB, which may explain why an *unc-7* mutation accelerates the onset of forward bias of the *jd1500* mutant phenotype when the animal attempts forward movement. Given our new knowledge regarding *jd1500*, it may be important to consider the AVB interneurons as a potential area of study surrounding this gene. Like the PVC, an ablation of AVB in *jd1500* may yield some important information.

One lab dissected AVB activity and found that AVB interneurons regulate the ability of the B motor neuron to generate a synchronous motor neurons circuit (Qi et. al., 2013). They observed a reduction in *acr-2(gf)* expression when they ablated AVB, which suggested that AVB is mediating B motor neuron activity (Qi et. al., 2013). They also found that *unc-7* and *unc-9* were not directly mediating B motor neuron *acr-2(gf)* activity, which was measured in convulsion frequency (Qi et. al., 2013). This was explained by the absence of *unc-7* and *unc-9* activating the backward motor neuron circuit when the animal attempted to move forward (Kawano et. al. 2011; Qi et. al., 2013). Confirming expression of *jd1500* in the interneurons AVB or B motor neurons could explain the asymmetrical biasing of *jd1500* animals as well. AVB interneurons drive both ventral and dorsal B motor neurons. If there is a defect in these interneurons, then one could expect differential locomotive disruption due to in interactions between these cells and the B motor neurons.

AVB has also been suggested to play a role in activating rhythm generators (Fouad et. al., 2018). We found that *jd1500* masked the phenotype of *acr-2*, which is one of the mutants implicated in proprioceptive feedback. These data suggest that *jd1500* is mediating at least one component of proprioceptive feedback. Given this result, the data suggests that gap junctions and

proprioceptive elements do not operate independent of each other, though our assay doesn't address how the two systems are linked. To further understand how these systems can interact with each other, there are a number of approaches that have proven valuable. One such approach is to use an optogenetic dissection of the involved locomotory systems. One lab used this approach and discovered that there is a distinct rhythmic linkage between anterior head bend frequency and tail bend frequency, termed 2FU (Fouad et. al., 2018). By disrupting this linkage using optogenetics, they were able to determine that the *C. elegans* locomotory activity is driven by multiple coupled "rhythm generating units" that work in tandem to produce the wave-like motion observed in animals (Fouad et. al., 2018).

In their study, they addressed whether *unc-7* and/or *unc-9* are required for this functional coupling to occur and found that both strains could still experience decoupling of anterior and posterior wave frequency (Fouad et. al., 2018). This suggests that neither is required to generate coupling in rhythmic units, though they found that AVB—which expresses *unc-7*—might be. Their reasoning for this discrepancy was that other premotor interneurons may attempt to "compensate for the loss of gap junctions between AVB and B neurons" (Fouad et. al., 2018). This data, when taken with Qi's data, suggests a model where AVB is directly responsible for forward locomotion and synchrony throughout the animal. Current evidence suggests that *unc-9* forms a heterotypic hemichannel with *unc-7* between the B motor neurons and AVB interneurons (Starich et. al., 2009). If *unc-7* and *unc-9* expression could be disrupted in AVB interneurons and B motor neurons without disrupting expression in the backward circuit, one might see reduction in synchrony of forward locomotion and in coupling of the rhythm generators. Our assay appears to categorize *jd1500* as a potential intermediary between the

pattern generators and the gap junctions. This must be explored further, and a combined genomic and optogenetic approach will further elucidate the position of *jd1500* in the locomotory system.

Within the same study, they concluded that rhythm generation is a unique feature of the B and possibly the AS motorneurons (Fouad et. al., 2018). Given that *jd1500* has been suggested in previous research to be a component of the B motor neurons and results here suggesting a role in gap junctions via the forward interneuron PVC, one could hypothesize that *jd1500* tested under the same conditions would lack 2FU. This would serve two purposes: to confirm whether the cellular networks impacted by *jd1500* also participate in rhythm generating units.

Rhythmic generators, or Central Pattern Generators, are not unique to *C. elegans*. Understanding the functional units of rhythm generators and how they interact with other locomotory systems within *C. elegans* can provide useful information with potential application in therapeutic areas of science. One such area is gene therapy for gait rehabilitation in genetic disorders. Current knowledge of central pattern generators suggests that gait is controlled rhythmically (Proske et. al., 2009; Gotschall et. al., 2007). If a link between rhythmic control of gait and gap junction activity is firmly established, new avenues of therapy addressing the gap junction side of locomotion can be developed. Coupling an intensive NGS PCR experiment with optogenetic manipulation of *jd1500* will provide valuable information about the link between rhythm generators and gap junction activity.

REFERENCES

1. Alcala, Aaron. “The genetic characterization of locomotive neural circuits is Caenorahabditis elegans.” Thesis. Georgia State University, 2016. N.p.: n.p., n.d.

2. Altun, Z. F., and D. H. Hall. "Nervous System, General Overview." *WormAtlas*. N.p., 19 June 2013.

3. Altun, Z. F., and D. H. Hall. "Handbook of *C. elegans* Anatomy." Wormatlas Homepage. N.p., 2012. Web.

4. Baran, R., R. Aronoff, and G. Garriga. "The *C. elegans* Homeodomain Gene Unc-42 Regulates Chemosensory and Glutamate Receptor Expression." *Development* 126 (1999): 2241-251.

5. Barnes, Thomas M., and S. Hekimi. "The Caenorhabditis Elegans Avermectin Resistance and Anesthetic Response Gene *Unc-9* Encodes a Member of a Protein Family Implicated in Electrical Coupling of Excitable Cells." Journal of Neurochemistry 69 (1997): 2251-260. Web.

6. Brenner, Sydney. "The Genetics of Caenorhabditis Elegans." *Genetics* 77 (1974): 71-94.

7. Bryden, John, and Netta Cohen. “Neural Control of Caenorhabditis Elegans Forward Locomotion: the Role of Sensory Feedback.” *Biological Cybernetics*, vol. 98, no. 4, 2008, pp. 339–351., doi:10.1007/s00422-008-0212-6.

8. Campbell, Nathan R., et al. “Genotyping-in-Thousands by Sequencing (GT-Seq): A Cost Effective SNP Genotyping Method Based on Custom Amplicon Sequencing.” *Molecular Ecology Resources*, vol. 15, no. 4, 2014, pp. 855–867., doi:10.1111/1755-0998.12357.

9. Chalfie, Martin, John E. Sulston, John G. White, Eileen Southdale, J. Nichol Thomson, and Sydney Brenner. "The Neural Circuit for Touch Sensitivity in Caenorhabditis Elegans." *The Journal of Neuroscience* 5.4 (1985): 956-64.

10. Celniker, Susan E. et al. “Unlocking the Secrets of the Genome.” Nature 459.7249 (2009): 927–930. PMC. Web. 11 Oct. 2017.

11. Driscoll, Monica. "Mechanotransduction." *C. elegans II. 2nd Edition.* U.S. National Library of Medicine, 01 Jan. 1997.

12. Enis Afgan, Dannon Baker, Marius van den Beek, Daniel Blankenberg, Dave Bouvier, Martin Čech, John Chilton, Dave Clements, Nate Coraor, Carl Eberhard, Björn Grüning, Aysam Guerler, Jennifer Hillman-Jackson, Greg Von Kuster, Eric Rasche, Nicola Soranzo, Nitesh Turaga, James Taylor, Anton Nekrutenko, and Jeremy Goecks. “The Galaxy platform for accessible, reproducible and collaborative biomedical analyses: 2016 update.” *Nucleic Acids Research* (2016) 44 (W1): W3-W10 doi:10.1093/nar/gkw343

13. Esmaeili, B., J. M. Ross, C. Neades, D. M. Miller, and J. Ahringer. "The *C. elegans* Even-skipped Homologue, *Vab-7*, Specifies DB Motoneurone Identity and Axon Trajectory." Development 129 (2002): 853-62.

14. Feng, Huiyun, John S. Reece-Hoyes, Albertha J.m. Walhout, and Ian A. Hope. "A Regulatory Cascade of Three Transcription Factors in a Single Specific Neuron, DVC, in Caenorhabditis Elegans." *Gene* 494.1 (2012): 73-84.

15. Fielenbach, N., and A. Antebi. "*C. elegans* Dauer Formation and the Molecular Basis of Plasticity." Genes & Development 22.16 (2008): 2149-165.

16. Fitzpatrick, D., et al. *Neuroscience.* 2nd ed., Sinauer Associates, 2001.

17. Foster, M., and C. S. Sherrington. *Textbook of Physiology*. 7th ed., vol. 3, Macmillan, 1897.

18. Fouad, Anthony D, et al. “Distributed Rhythm Generators Underlie Caenorhabditis Elegans Forward Locomotion.” ELife, vol. 7, 2018, doi:10.7554/elife.29913.

19. Gottschall, Jinger S., and T. Richard Nichols. "Head Pitch Affects Muscle Activity in the Decerebrate Cat Hindlimb during Walking." Experimental Brain Research 182.1 (2007): 131-35. Web.

20. Hu, Xinge, and Gerhard Dahl. "Exchange of Conductance and Gating Properties between Gap Junction Hemichannels." FEBS Letters 451.2 (1999): n. pag. Web.

21. Kawano, Taizo, Michelle D. Po, Shangbang Gao, George Leung, William S. Ryu, and Mei Zhen. "An Imbalancing Act: Gap Junctions Reduce the Backward Motor Circuit Activity to Bias *C. elegans* for Forward Locomotion." *Neuron* 72.4 (2011): 572-86.

22. Li, Wei, Zhaoyang Feng, Paul W. Sternberg, and X. Z. Shawn Xu. "A *C. elegans* Stretch Receptor Neuron Revealed by a Mechanosensitive TRP Channel Homologue." Nature 440.7084 (2006): 684-87.

23. Li, Wenli, et al. “Comprehensive Evaluation of AmpliSeq Transcriptome, a Novel Targeted Whole Transcriptome RNA Sequencing Methodology for Global Gene Expression Analysis.” *BMC Genomics*, vol. 16, no. 1, 2015, doi:10.1186/s12864-015-2270-1.

24. Mclntire, Steven L., Erik Jorgensen, Joshua Kaplan, and H. Robert Horvitz. "The GABAergic Nervous System of Caenorhabditis Elegans." *Nature* 364.6435 (1993): 337-41.

25. Miller, David M., Michael M. Shen, Caroline E. Shamu, Thomas R. BÃ¼rglin, Gary Ruvkun, Michelle L. Dubois, Medeva Ghee, and Laura Wilson. "*C. elegans* Unc-4 Gene Encodes a Homeodomain Protein That Determines Thepattern of Synaptic Input to Specific Motor Neurons." *Nature* 355.6363 (1992): 841-45.

26. Oommen, K.S. "Behavioral, structural, and genetic analyses of *unc-jd19*, a gene affecting the DD inhibitory motoneurons in *Caenorhabditis elegans*." Thesis. Georgia State University, 1999. N.p.: n.p., n.d.

27. Phelan, Pauline, and Todd A. Starich. "Innexins Get into the Gap." BioEssays. John Wiley & Sons, Inc., 30 Apr. 2001. Web.

28. Prochazka, Arthur, and Sergiy Yakovenko. "The Neuromechanical Tuning Hypothesis." Progress in Brain Research Computational Neuroscience: Theoretical Insights into Brain Function (2007): 255-65. Web.

29. Proske, Uwe, and Simon C. Gandevia. "The Kinaesthetic Senses." The Journal of Physiology 587.17 (2009): 4139-146. Web.

30. Qi, Y. B., et al. "Hyperactivation of B-Type Motor Neurons Results in Aberrant Synchrony of the Caenorhabditis Elegans Motor Circuit." *Journal of Neuroscience*, vol. 33, no. 12, 2013, pp. 5319–5325. doi:10.1523/jneurosci.4017-12.2013.

31. Rakowski, Franciszek, et al. "Synaptic Polarity of the Interneuron Circuit Controlling C. Elegans Locomotion." *Frontiers in Computational Neuroscience*, vol. 7, 2013, doi:10.3389/fncom.2013.00128.

32. Spencer, W. C., G. Zeller, J. D. Watson, S. R. Henz, K. L. Watkins, R. D. Mcwhirter, S. Petersen, V. T. Sreedharan, C. Widmer, J. Jo, V. Reinke, L. Petrella, S. Strome, S. E. Von

Stetina, M. Katz, S. Shaham, G. Ratsch, and D. M. Miller. "A Spatial and Temporal Map of *C. elegans* Gene Expression." Genome Research 21.2 (2010): 325-41.

33. Starich, Todd A., Robert K. Herman, and Jocelyn E. Shaw. "Molecular and Genetic Analysis of *Unc-7*, a Caenorhabditis Elegans Gene Required for Coordinated Locomotion." Genetics. U.S. National Library of Medicine, Mar. 1993. Web.

34. Starich, Todd A, et al. "Interactions between Innexins *UNC-7* and *UNC-9* Mediate Electrical Synapse Specificity in the Caenorhabditis Elegans Locomotory Nervous System." *Neural Development*, vol. 4, no. 1, 2009, p. 16. doi:10.1186/1749-8104-4-16.

35. Stein, L. "WormBase: Network Access to the Genome and Biology of Caenorhabditis Elegans." *Nucleic Acids Research* 29.1 (2001): 82-86.

36. The *C. elegans* Sequencing Consortium "Genome Sequence of the Nematode *C. elegans*: A Platform for Investigating Biology." Science (New York, N.Y.). U.S. National Library of Medicine, 11 Dec. 1998. Web.

37. Wen, Quan, Michelle D. Po, Elizabeth Hulme, Sway Chen, Xinyu Liu, Sen Wai Kwok, Marc Gershow, Andrew M. Leifer, Victoria Butler, Christopher Fang-Yen, Taizo Kawano, William R. Schafer, George Whitesides, Matthieu Wyart, Dmitri B. Chklovskii, Mei Zhen, and Aravinthan D.t. Samuel. "Proprioceptive Coupling within Motor Neurons Drives *C. elegans* Forward Locomotion." *Neuron* 76.4 (2012): 750-61.

38. White, J. G., E. Southgate, J. N. Thomson, and S. Brenner. "The Structure of the Ventral Nerve Cord of Caenorhabditis Elegans." *Philosophical Transactions of the Royal Society B: Biological Sciences* 275.938 (1976): 327-48.

39. Ziel, Joshua W., David Q. Matus, and David R. Sherwood. "An Expression Screen for RhoGEF Genes Involved in *C. elegans* Gonadogenesis." Gene Expression Patterns 9.6 (2009): 397-403. Web.

40. Zheng, Chaogu, Margarete Diaz-Cuadros, and Martin Chalfie. "GEFs and Rac GTPases Control Directional Specificity of Neurite Extension along the Anterior–posterior Axis." *Proceedings of the National Academy of Sciences of the United States of America*. National Academy of Sciences, 21 June 2016.

APPENDIX

Table 2 P-values for Proprioceptive mutants coil frequency comparisons. Bold indicated One-Way ANOVA. '>' indicated Student T-Test. If ANOVA P-value was less than 0.05, t-tests were deployed.

Strains	**P-value**
jd1500 - acr-2 - jd1500 acr-2	0.0002
>jd1500 - acr-2	0.0001
>jd1500 - jd1500 acr-2	0.764
>acr-2 - jd1500 acr-2	0.0002
jd1500 - trp-4 - jd1500; trp-4	0.849
jd1500 - vab-7 - jd1500; vab-7	0.042
>jd1500 - vab-7	0.033
>jd1500 - jd1500; vab-7	0.346
>vab-7 - jd1500; vab-7	0.055

Table 3 DV ratio values for Proprioceptive mutants vs jd1500.

Strains	**0**	**0.25**	**0.5**	**0.75**	**1**
jd1500	0.95006588	1.06600963	0.79174818	0.51112384	0.414624546
jd1500 acr-2	1.06472919	0.78883816	0.53064651	0.46325570	0.747690941
acr-2	0.96740052	1.22675487	0.99447233	0.89502763	0.918055177
jd1500; trp-4	1.02199202	1.21007937	0.85090525	0.54716065	0.594813923
trp-4	1.14043737	1.02279408	0.47310259	0.3604381	0.683420434

Table 4 P values for Proprioceptive Mutant DV ratios. Student T-tests were used.

Strain	**0**	**0.25**	**0.5**	**0.75**	**1**
jd1500 - acr-2	0.921	0.497	0.223	0.003	0.001
jd1500 - jd1500 acr-2	0.599	0.124	0.11	0.689	0.071
acr-2 - jd1500 acr-2	0.633	0.048	0.0006	0.0002	0.322
jd1500 - trp-4	0.332	0.891	0.0062	0.355	0.146
jd1500 - jd1500; trp-4	0.689	0.547	0.712	0.776	0.189
trp-4 - jd1500; trp-4	0.519	0.579	0.006	0.229	0.598

Table 5 P-values for Innexin mutants coil frequency comparisons. Bold indicated One-Way ANOVA. '>' indicated Student T-Test. If ANOVA P-value was less than 0.05, t-tests were deployed.

Strains	P-value
jd1500 - unc-7 - jd1500 unc-7	0.0002
>jd1500 - unc-7	0.012
>jd1500 - jd1500 unc-7	0.023
>unc-7 - jd1500 unc-7	0.431
jd1500 - unc-9 - jd1500 unc-9	0.0003
>jd1500 - unc-9	0.012
>jd1500 - jd1500 unc-9	0.0007
>unc-9 - jd1500 unc-9	0.007

Table 6 DV ratio values for Innexin mutants vs jd1500.

Strains	0	0.25	0.5	0.75	1
jd1500	0.950065886	1.066009631	0.791748183	0.511123845	0.414624546
jd1500 unc-7	1.362171335	0.552455219	0.483801115	0.522213528	0.890897694
unc-7	1.038139336	0.984213952	1.0266231	0.742780276	0.884918298
jd1500 unc-9	0.833775992	1.018977077	0.8119037	0.849252845	0.741233028
unc-9	1.01332936	0.936752789	0.868133366	0.907856885	0.904955063

Table 7 P values for Innexin Mutant DV ratios. Student T-tests were used.

Strain	**0**	**0.25**	**0.5**	**0.75**	**1**
jd1500 - unc-7	0.751	0.632	0.217	0.054	0.001
jd1500 unc-7 - jd1500	0.418	0.007	0.076	0.929	0.036
unc-7 - jd1500 unc-7	0.55	0.002	0.003	0.025	0.976
jd1500 - unc-9	0.719	0.502	0.703	0.004	0.0023
jd1500 unc-9 - jd1500	0.529	0.806	0.905	0.014	0.021
unc-9 - jd1500 unc-9	0.293	0.637	0.75	0.587	0.207

Table 8 DV ratio values for Innexin controls.

Strains	**0**	**0.25**	**0.5**	**0.75**	**1**
unc-7	1.038139336	0.984213952	1.0266231	0.742780276	0.8849182
unc-7; unc-30	0.927885746	0.790750836	0.58482959	0.641484727	0.6001680
unc-9	1.01332936	0.936752789	0.868133366	0.907856885	0.9049550
unc-9; unc-30	1.097082818	1.117621852	0.862333647	0.614023028	0.5875847
unc-30	0.984747958	0.913971761	0.619902491	0.594835748	0.6762852

Table 9 P values for Innexin controls. Bold indicated One-Way ANOVA. '>' indicated Student T-Test. If ANOVA P-value was less than 0.05, t-tests were deployed.

Strains	**0**	**0.25**	**0.5**	**0.75**	**1**
unc-7 - unc-7; unc-30 - unc-30	0.083	0.333	0.031	0.447	0.04
>unc-7 - unc-30			0.23		0.051
>unc-7 - unc-7; unc-30			0.043		0.034
>unc-30 - unc-7; unc-30			0.85		**0.523**
unc-9 - unc-9; unc-30 - unc-30	0.841	0.744	0.268	0.034	0.027
>unc-9 - unc-30				0.031	0.07
>unc-9 - unc-9; unc-30				0.008	0.016
>unc-30 - unc-9; unc-30				0.882	0.364